Characteristics of fluorinated amorphous carbon films and implementation of 0.15 m Cu /a- C:F damascene interconnection

Jia-Min Shieh, Shich-Chang Suen, Kou-Chiang Tsai, Bau-Tong Dai, Yew-Chung Wu, and Yu-Hen Wu

Citation: Journal of Vacuum Science & Technology B **19**, 780 (2001); doi: 10.1116/1.1362683
View online: http://dx.doi.org/10.1116/1.1362683
View Table of Contents: http://scitation.aip.org/content/avs/journal/jvstb/19/3?ver=pdfcov
Published by the AVS: Science & Technology of Materials, Interfaces, and Processing

Characteristics of fluorinated amorphous carbon films and implementation of 0.15 μm Cu/*a*-C:F damascene interconnection

Jia-Min Shieh,[a] Shich-Chang Suen, Kou-Chiang Tsai, and Bau-Tong Dai
National Nano Device Laboratories, Hsinchu 30050, Taiwan

Yew-Chung Wu and Yu-Hen Wu
Institute of Materials Science and Engineering, National Chiao Tung University, Hsinchu 30050, Taiwan

(Received 6 October 2000; accepted 12 February 2001)

Fluorinated amorphous carbon films (*a*-C:F) deposited by plasma enhanced chemical vapor deposition with low dielectric constant ($K \sim 2.3$), thermal stability (higher than 400 °C) and acceptable adhesion to a cap layer such as SiOF or SiO_2 were obtained by varying the range of content ratios between carbon and fluorine, the rf power, the process pressure and the base temperature. Standard x-ray photoelectron spectroscopy and thermal desorption spectroscopy metrologies were employed to characterize the deposited *a*-C:F films. The damascene pattern with 0.15 μm and an etching selectivity of more than 50 (*a*-C:F/SiOF, SiO_2) was implemented by a mixture of etching gases of N_2+O_2. The bias power, rf power and gas flows were incorporated to optimize the etching recipe for achieving a damascene profile with a high aspect ratio. The scanning electron microscope results showed that a better etch profile can be obtained at higher bias power. In our damascene architecture, the etching stop layer or hard mask of both SiOF and SiO_2 was studied. The SiOF, providing a lower dielectric constant than SiO_2, would especially reduce the entire effective dielectric constant. Furthermore, we integrated electroplated copper into trenches or vias as small as 0.15 μm, with aspect ratio of 6. © *2001 American Vacuum Society.*
[DOI: 10.1116/1.1362683]

I. INTRODUCTION

The dual damascene structure for integrating electroplating copper as a metal line and low-*K* material as an inter- or intralayer for ultralarge-scale integrated (ULSI) chips has imposed intense industry-wide efforts on developing a novel process and material and integration technology. Up to now, copper electroplating technology for 0.13 μm damascene has been exploited and many research groups and manufacturers have reported their results.[1–3] The next challenge for metallization is copper integrating with low-dielectric constant materials. For now, these low-*K* dielectrics can be classified as organic and inorganic polymers, and can be deposited by either chemical vapor deposition (CVD) or spin-on techniques.[4] For instance, fluorinated amorphous carbon (*a*-C:F)[5,6] films were deposited by plasma enhanced chemical vapor deposition (PECVD), and polyimide[4] and hydrogen silsesquioxane (HSQ)[7] films were deposited by spin coating. In the future, a dielectric constant lower than 2.0 should introduce new materials or processes such as dielectric films with porous structures.[8] Although there were many candidates for low-dielectric constant materials, the CVD-based material has still played a more important role up to now because a minor change in the integral processes could be met as expected. Both black-diamond S–C films[9] and *a*-C:F films are two major materials that have been successfully deposited by traditional PECVD equipment. The precursors for the former was trimethylsilane or similar derivatives (Z3MS),[9] the mixture gases including carbon and fluorine atoms were precursors for fluorinated amorphous carbon films (*a*-C:F). Those two low-*K* films were able to provide reliable and acceptable features especially since their dielectric constants were below 2.5, better than conventional spin-on-based low-*K* materials. Although for porous silica, with an ultralow dielectric constant, the thermal conductivity was typically several tens to hundreds times of poorer than S–C or *a*-C:F films. Because the *a*-C:F film could be deposited by conventional PECVD without changing equipment and had the acceptable properties mentioned, this material became the focus for a candidate of low-*K* materials. In fact, there has been much investigative work on *a*-C:F. Ma *et al.* discussed[10] the effect of the deposition temperature on thermal and dielectric constant aspects of *a*-C:F. Detailed material analyses of *a*-C:F through x-ray photoelectron spectroscopy (XPS) and Fourier-transform infrared (FTIR) spectra have been implemented.[11] Effects of process pressure for the same questions were reported by the Endo groupe.[12] In reviewing most of those investigations, optimization between process parameters and even integral issues with sequential process was lacking.

The electrical, chemical, mechanical, and thermal properties must be considered for all low-*K* materials and they must be compatible with other processes (e.g., photolithography and etching). But when the device feature size continues to scale down, dielectric etching processes face a challenge. One key issue is a deficient etching selection ratio between the organic-based low-*K* material with photoresist. An etching stop layer should be introduced to overcome this difficulty. Due to such an arrangement, the effective dielectric constant was enlarged. Finding a suitable etching stop layer

[a]Corresponding author; electronic mail: imshieh@ndl.gov.tw

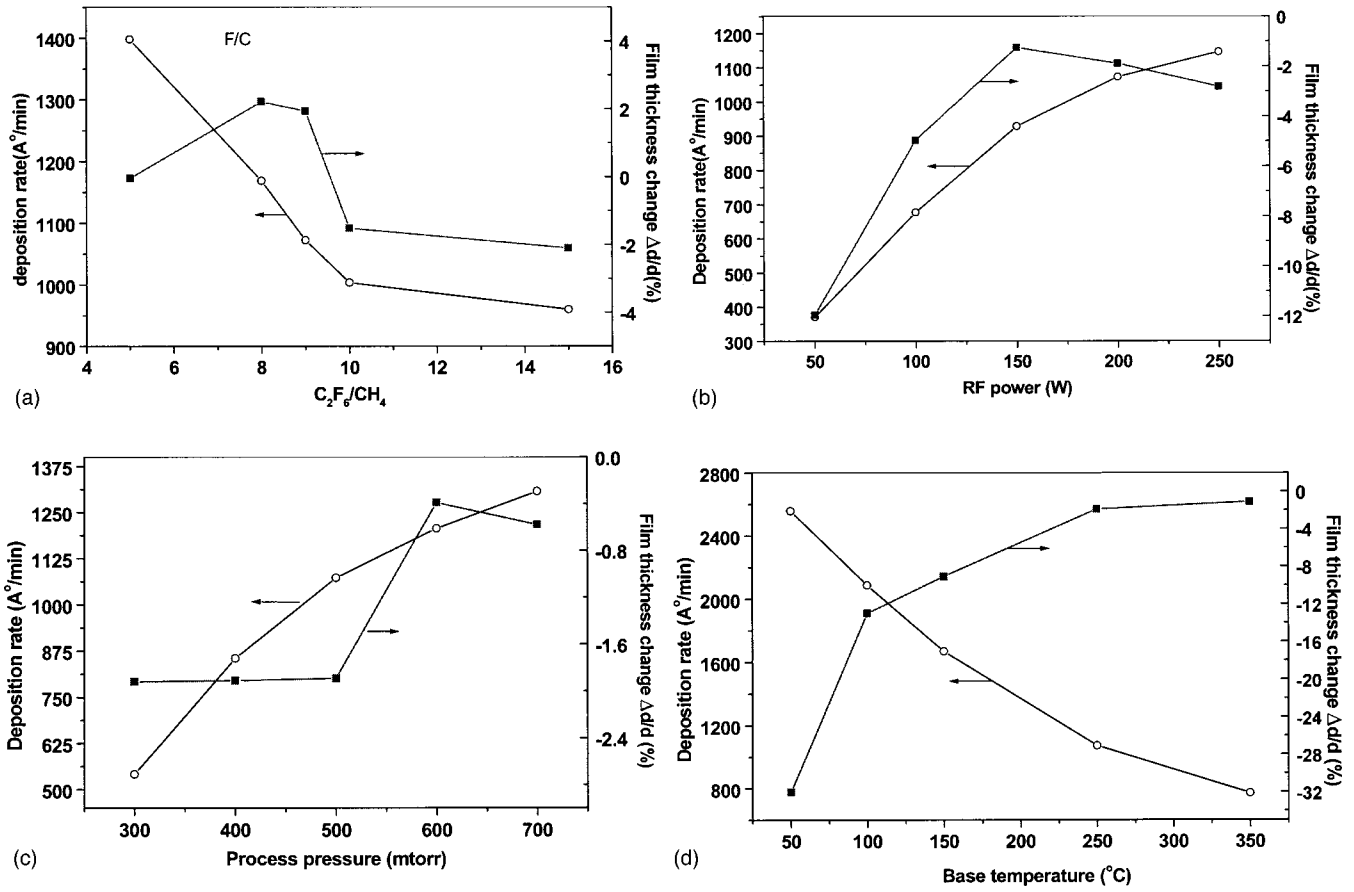

FIG. 1. Deposition rate and film thickness changes after annealing at 400 °C for 300 min as functions of various process parameters: (a) C_xF_y/CH_4 ratio, (b) plasma power, (c) process pressures, and (d) base temperature.

with the properties mentioned became more and more important. Another issue about etching Damascene with a high aspect ratio was that etching reactant gases must provide the passivation effect on sidewall surfaces for an increased anisotropic etching rate.[13,14] Breen *et al.*[15] proposed that addition of polymerizing components to the etch chemistry could suppress the isotropic component. The undesired polymer residues might become more difficult to remove since the addition of reaction gases generally consisted of carbon–fluorine–hydrogen-based gases (C_xF_y, CH_xF, C_xH_y) and their chemical features are very similar to underlayer low-K materials.[15] For the low-dielectric material, a-C:F, in which we are interested contents of carbon and fluorine existed in the materials. Here, we examine the etching recipe, combining a mix of gases of chemical etch gas (such as oxygen), diluted in the bombarded etch gas nitrogen gas. Such an arrangement could provide a different passivation layer, C_xN_y, from a-C:F.

In the present work, fluorinated amorphous carbon films (a-C:F) were deposited by PECVD. By optimizing the content ratio between carbon and fluorine, rf power, process pressure, and base temperature, optimized amorphous carbon films (a-C:F) which have low-dielectric constant ($K \sim 2.3$), thermal stability (higher than 400 °C), are electrically insulating, have high mechanical strength, and acceptable adhesion to a cap layer such as SiO_2 or SiOF were deposited. The leakage could be controlled below 2.0×10^{-8} A/cm^2. The stress for all deposited a-C:F films was below -35 MPa. The shrinkage of the deposited films after 400 °C, 30 min annealing was below 2.0%. The dynamics for the thermal stability, dielectric constant, and current leakage were investigated by analyzing thermal desorption spectroscopy (TDS) and XPS spectra. The damascene pattern with 0.15 μm and an etching selection ratio of more than 50 (a-C:F/SiOF, SiO_2) was implemented by an etching gas mixture of N_2+O_2. The bias power, rf power, and gas flows were incorporated to optimize the etching recipe to achieve a damascene profile with a high aspect ratio. In our Damascene architecture, the etching stop layer or hard mask of both SiOF and SiO_2 was employed. SiOF, providing a lower dielectric constant than SiO_2, would especially, reduce the entire effective dielectric constant. Furthermore, we integrated electroplated copper into trenches or vias as small as 0.15 μm, with aspect ratio (AR) of 6.

II. FUNDAMENTAL CHARACTERISTICS OF *a*-C:F FILMS

Fluorinated amorphous carbon films (a-C:F) were deposited by PECVD. The basic precursor gas is a mixture of CH_4

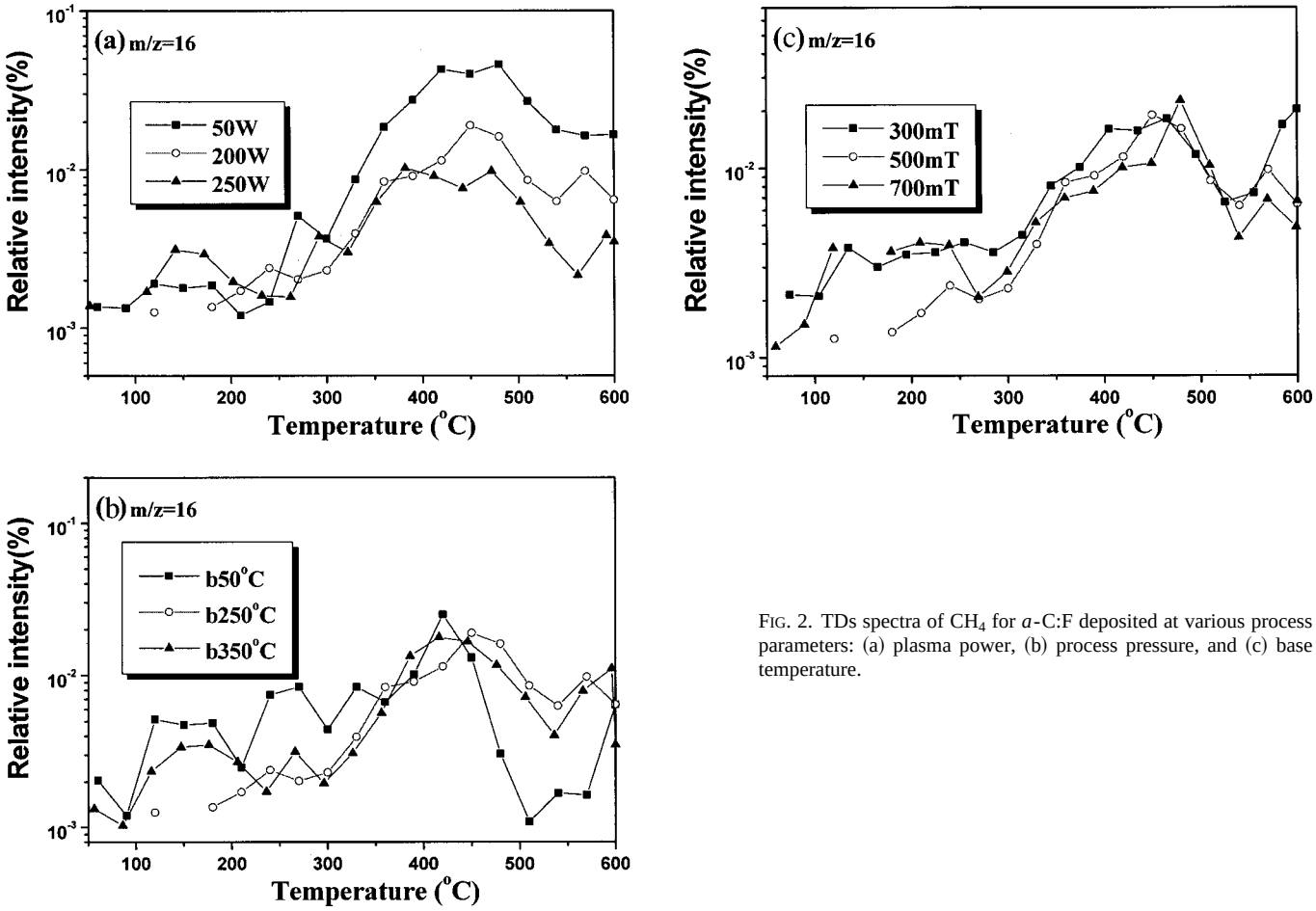

FIG. 2. TDs spectra of CH_4 for *a*-C:F deposited at various process parameters: (a) plasma power, (b) process pressure, and (c) base temperature.

and C_2F_6. The thickness and refractive index of those films were measured by a N&K analyzer 1200. Thermal stability was examined by curing the deposited *a*-C:F films in a furnace at 400 °C for 30 min in N_2 ambient at a flow rate of 10 l/min. X-ray photoelectron spectroscopy was used to measure the C 1*s* x-ray photoelectron spectrum, and provided detailed information on the local bonding environment of carbon atoms. Since the peaks in the spectra represent carbon atoms in C–F, $C–F_2$, $C–F_3$, C–(C, H), C–CF bonding environments, the peak height denotes characteristics of *a*-C:F. TDS was used to measure the degree of desorption of different bonding classes (such as CH_4, H_2O, CF_x) of the *a*-C:F films as a function of temperature to compare mechanisms of process parameters on the thermal stability and moisture resistivity. Adhesion was judged by the degree of peeling off after 3M tape tests. To evaluate the etching characteristics such as the etch rate, profile, and selectivity, three types of 6 in. wafers were used. The three types were blank SiO_2 SiOF, blank *a*-C:F, and patterned *a*-C:F. Then, a 50 nm silicon oxide mask was patterned by electron-beam lithography (smallest feature=0.15 μm). All three types of wafer were etched in a helicon-wave plasma etching system (ANELVA ILD-4100) with a photomultiplier tube (PMT) MØRI™ 200 helicon plasma source. Radio frequency power of 13.56 MHz was used to generate the plasma and additional 13.56 MHz rf power provided the bias with which to control the ion bombardment energy. The bias power was varied from 0 to 90 W. N_2 and O_2 were used at a total flow rate of 100 sccm. Etch results were examined by scanning electron microscopy (SEM). Plasma etching was controlled by three mechanisms: physical bombardment, chemical etching, and chemical passivation.[16,17] Selective and anisotropic etching can be achieved by a good balance of the above three processes.

Figures 1(a)–1(d) show the deposition rates and shrinkage of *a*-C:F as functions of the C_xF_y/CH_4 ratio, rf power, process pressure, and base temperature. Since the etching behavior induced by fluorine atoms would become apparent when the content of CH_4 in the reactant gas decreases, the deposition rate decreases by the higher C_xF_y/CH_4, as shown in Fig. 1(a). Because the higher rf power and process pressure enhance the deposition rate, the experimental data in Figs. 1(b) and 1(c) are in agreement with such deductions. Figure 1(d) shows the slower deposition rate under a higher base temperature. This phenomenon has been observed in the Endo group's research.[12] The viscosity of the reactant species is inversely proportional to the process temperature. Based on this dynamic, the deposition rate should become slow if the high temperature effect weakened the adsorption coefficient between the deposited substrate and the precursor gases. In this work, we found that the annealing test of thickness shrinkage was almost unaffected in the wide range of differ-

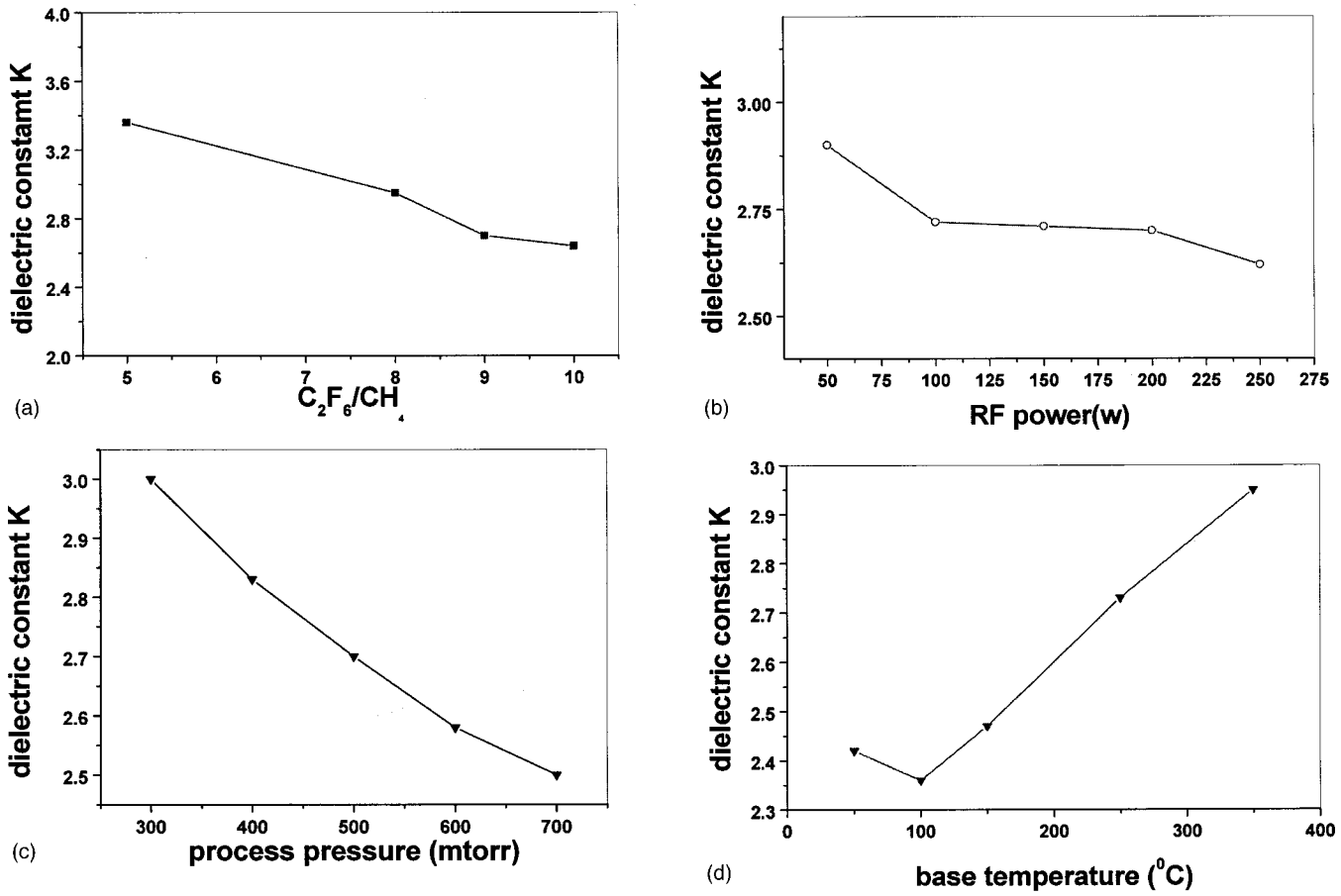

FIG. 3. Dielectric constant ϵ_s as function of the deposition parameters: (a) C_xF_y/CH_4 ratio, (b) plasma power, (c) process pressures, and (d) base temperature.

ent C_xF_y/CH_4 ratios [Fig. 1(a)] and process pressures [Fig. 1(c)]. This tolerance of the process window for the thermal stability became very critical when the plasma power [Fig. 1(b)] and base temperature [Fig. 1(d)] were considered. At a higher process temperature or plasma power, the film shrinkage (thermal stability) was less than 5% when the plasma power and process temperature were above 150 W and 200 °C. With regard to the effects of process pressure and C_xF_y/CH_4 ratio, the film shrinkage was below 2% in the whole process range. The effect of the C_xF_y/CH_4 ratio on the thermal stability was similar to that in previous work.[12,18] Because the higher rf power and process pressure form a more densely deposited film, the change of film thickness was typically unaffected by the annealing process.[19,20] Our *a*-C:F films demonstrated quite good thermal stability in the wide range of process pressures without the high process pressure limitation. According to the degree of film shrinkage shown in Figs. 1(a)–1(d), the thermal stability of the deposited *a*-C:F film could attain 400 °C.

In general, fluorine atoms neighboring carbon atoms and forming $C–F_x$ were proposed as contributing to the electrical performance and C–C crosslinked structure, maintaining the film's thermal stability.[12] Consequently, we could examine the degree of CH_4 desorption from *a*-C:F deposited at different process parameters, then exploit their mechanisms. TDS spectra of CH_4 for different plasma powers showed more desorption abundance from *a*-C:F deposited at low plasma power, as shown in Fig. 2(a). Since Fig. 2(b) shows spectra for a different base temperature, we noticed more desorption abundance from *a*-C:F deposited at room temperature. There were some significant differences for TDS spectra representing different process pressures, such as spectral curves overlapping, as shown in Fig. 2(c). Since the TDS data showed more of a minor effect of process pressure on CH_4 desorption than temperature and plasma power, the corresponding thermal stability affected by process pressure became unimportant. The optimum parameters are in the range of $C_xF_y/CH_4 \sim 10$, rf plasma power of ~200 W, process pressure of ~550 mTorr, and deposition temperature of ~250 °C. The total gas flow employed for depositing *a*-C:F is 300 sccm. The deposition rate is typically $R_d = 1000$ Å/min, film shrinkage is less than 2.0%, and the stress for all deposited *a*-C:F films is below −35 MPa.

To determine the dielectric constant and leakage current of those low-*K* films, metal–insulator–semiconductor (MIS) (Al/low-*K* film/p^+Si) capacitor structures were made. The area of the aluminum dot for electrical feature measurements was 5.0×10^{-3} cm^2. The electrical characteristics of *a*-C:F

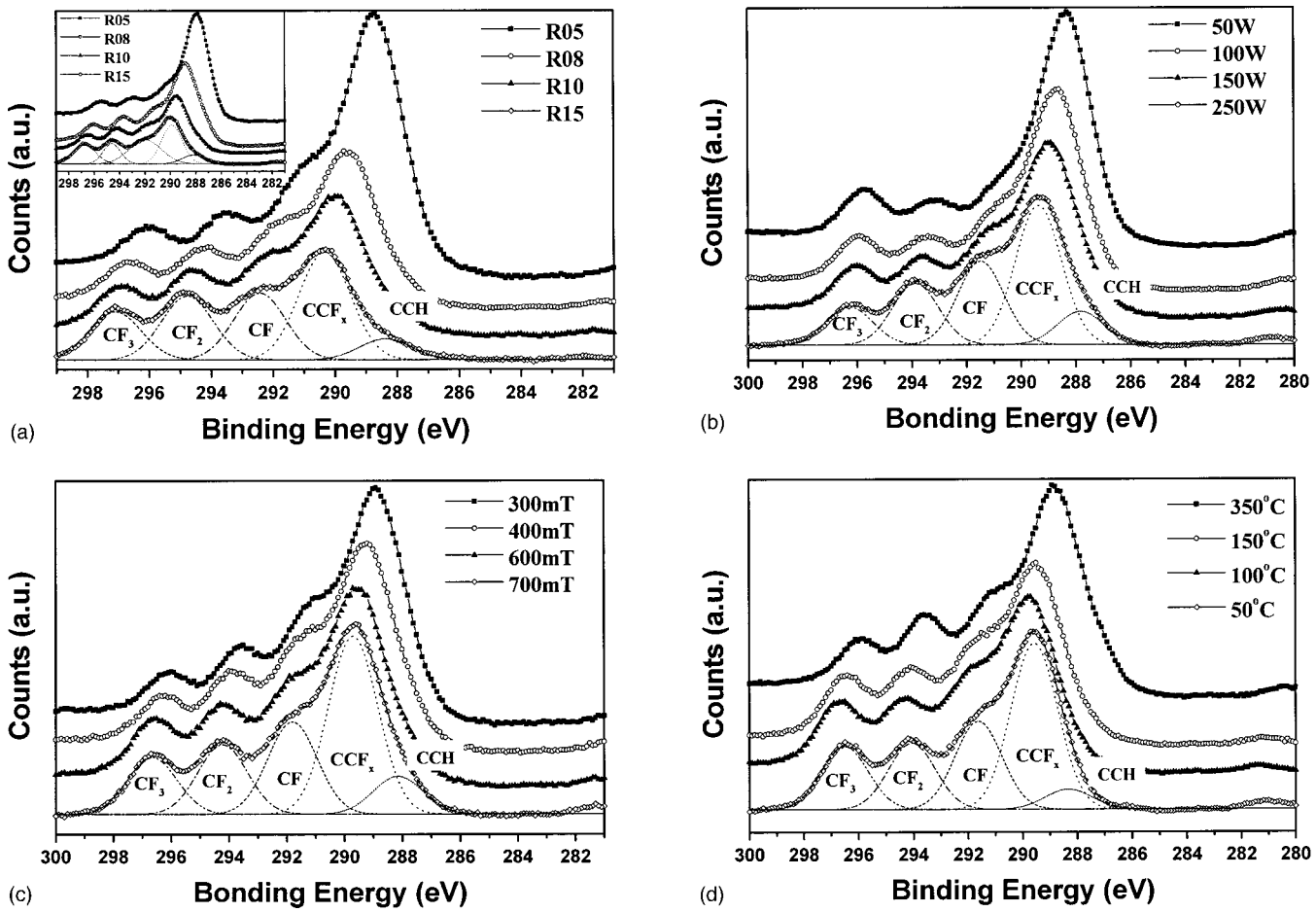

FIG. 4. XPS C 1*s* spectra for *a*-C:F deposited with various process parameters: (a) C_xF_y/CH_4 ratio, (b) plasma power, (c) process pressures, and (d) base temperature.

films are functions of the process pressure, the content ratio between carbon and fluorine, plasma power, etc. In our experimental results, the dielectric constant reduced as the C_xF_y/CH_4, plasma power, and process pressure increased, shown in Figs. 3(a)–3(c). Conversely, the dielectric constant of *a*-C:F deposited at the higher temperature was higher, shown in Fig. 3(d). XPS spectra for different C_xF_y/CH_4 ratios, shown in Fig. 4(a), demonstrated that the relative abundance of C^*F_3, C^*F_2 became higher than C^*-CF_x because the F/C ratio was increased by the addition of more C_xF_y. This means that more carbon atoms without directly bonded fluorine existed in the *a*-C:F films if more CH_4 was added. Consequently, fewer C–F bonds would cause the dielectric constant to be higher. Higher plasma and process pressure deposited *a*-C:F films with more $C–F_x$ are verified by Figs. 4(b) and 4(c). Figure 4(d) shows the *a*-C:F films with more $C–F_x$ at room temperature.

The typical dielectric constant is $K=2.6$, and the minimum value is as low as $K=2.3$ when the deposition parameters include process pressure of ~700 mTorr and C_2F_6/CH_4 of ~10 under loss of adhesion quality and thermal stability. If the dielectric constant $K=2.5$ of *a*-C:F films was prepared using various process parameters, the leakage could be controlled to about $I_d \approx 2.0\times10^{-8}/\text{cm}^2$ at bias electric field of $E_{\text{bias}}=1.0$ MV/cm, shown in Figs. 5(a)–5(d). The electrical characteristics remaintained unchanged after 400 °C thermal annealing. In general, an electron was more difficult to transfer to the conduction band if there were more C–F bonds in the *a*-C:F, since the F atoms provided stronger attraction to electrons. Actually, the energy gap E_g increasing from 2.72 to 3.44 eV when the C_xF_y/CH_4 ratio increased from 5 to 15 verified this concept. Figure 5(a) shows a reduction trend of current leakage I_g for higher C_xF_y/CH_4. Although higher plasma power and process pressure resulted in *a*-C:F with a higher F/C ratio, the current leakages inversely increased without the mechanisms described above. The phenomenon was proposed because more activation sites generated during the deposition process under high plasma power or process pressure became transportation agents of free electrons to conduction bands. Furthermore, we have mentioned that *a*-C:F films deposited in a high temperature environment allowed reaction radials to escape easily, and this would form a film structure with unsaturated bonds and lower the energy gap E_g. According to these dynamics, the deposited *a*-C:F films with high leakage current were obtained under a high base temperature condition.

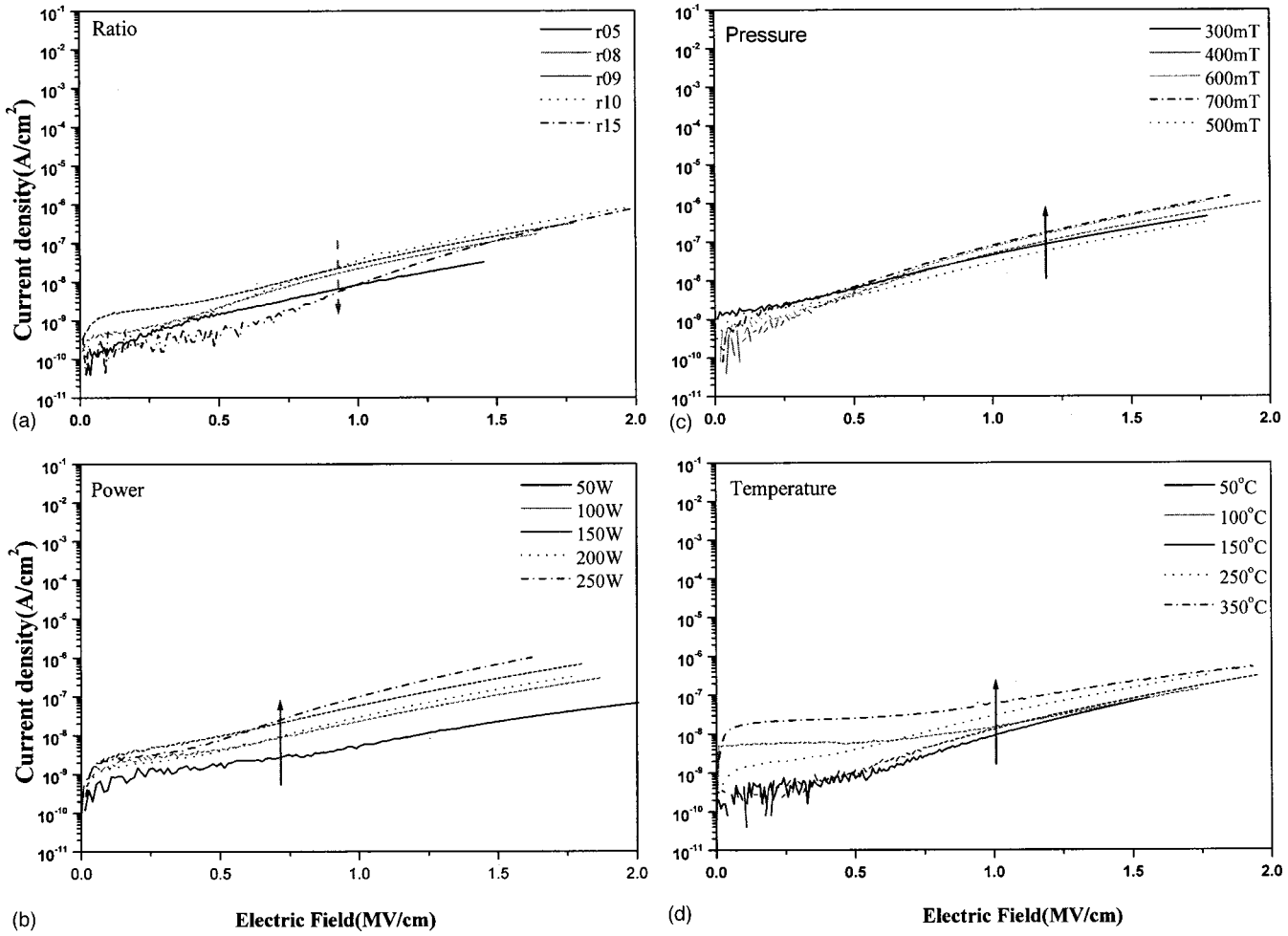

FIG. 5. Leakage currents as functions of the deposition parameters: (a) C_xF_y/CH_4 ratio, (b) plasma power, (c) process pressures, and (d) base temperature.

III. METALLIZATION OF COPPER/LOW-*K* INTERCONNECT

The etching rates of *a*-C:F for various parameters including the gas flow ratio and bias power were investigated. Figure 6 shows the etch rates of *a*-C:F with N_2 addition to O_2 plasmas. The N_2 addition diluted the available oxygen molecules, which diminished the etch rate of *a*-C:F and hence its selectivity to SiO_2. In the range of N_2/O_2 gas flow ratios below 80/20, the etching rates of *a*-C:F and SiO_2 were above 7000 and 100 Å/min, respectively, while the etching selectivity was more than 50. The other etching parameters were bias power of 60 W, rf power of 2000 W, temperature of ~60 °C, total gas flow rate of ~100 sccm, and pressure of ~5 mTorr. Figure 7 shows the etch rates of *a*-C:F and SiO_2

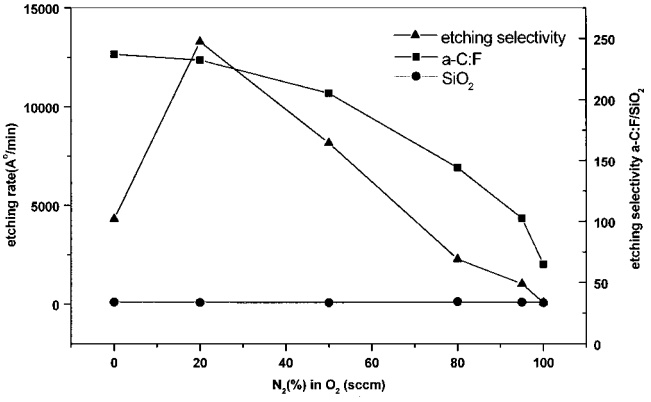

FIG. 6. Variation of the SiO_2 etch rate, dielectric etch rate, and dielectric/SiO_2 selectivity with the relative N_2 in O_2 percentage.

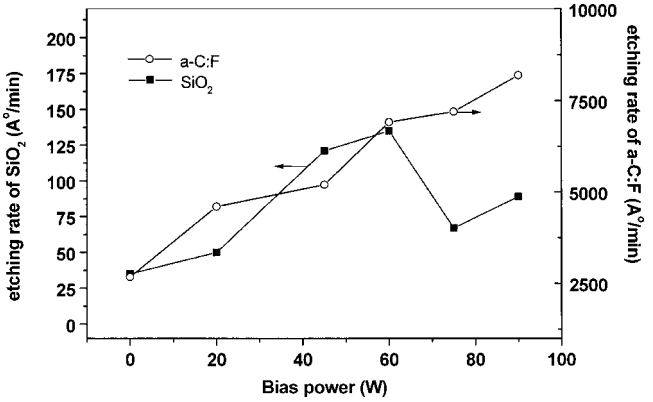

FIG. 7. Variation of the SiO_2 etch rate and dielectric etch rate with bias power (N_2 and O_2 as etchant gases).

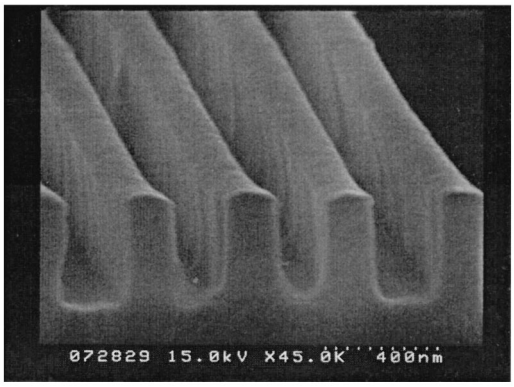

FIG. 8. SEM images of the etching profiles of *a*-C:F in $N_2/O_2=80/20$ (total gas flow rate of 100 sccm), bias power of 60 W, and plasma power of 2000 W (60 s, 0.15 μm pattern).

with the bias power varying from 0 to 90 W. While the etch rate of *a*-C:F increases monotonically with bias power, there are nearly no changes in the oxide etch rate. This suggests that the etching of *a*-C:F in high density plasmas is ion enhanced. The SEM image of the etching profiles of *a*-C:F in N_2/O_2 etching gases demonstrated a perfectly vertical 0.15 μm damascene pattern, shown in Fig. 8. The pattern width was close to 150 nm, and the thickness of the *a*-C:F and SiO_2 films was about 500 and 500 nm, respectively. The complete parameters for etching *a*-C:F and SiO_2 are listed in Table I. Sidewall passivation provided by nitrogen gases has successfully formed a C_xN_y layer, without the cost of removing the polymerizing passivation layer selective to *a*-C:F as carbon–fluorine–hydrogen-based additive gases (C_xF_y, CH_xF, C_xH_y). This is quite important for integration with subsequent metallization. Severe undercutting was seen in the SEM image of the etching profiles of *a*-C:F in pure oxygen plasma because the anisotropic etching was not strong enough to maintain vertical etching profiles since a moderate passivation layer was lacking, as shown in Fig. 9. The processing time T_{etch} for *a*-C:F was 60 s. Calculating the etched depth of *a*-C:F from SEM images, it is found that the etching rate is about 4000 Å/min. As the data of the etching rate for blanket *a*-C:F, the process time T_{etch} could etch the depth of the film more than 7000 Å/min. There was some deviation between the etching rate of the blanket with the patterned wafer. The major reason was that the distribution density of the reactant etching gas in the sub-μm gap was quite different from the blanket surface of the wafer. Due to this phenomenon, the process time T_{etch} became a nonlinear function of linewidth and depth.

Basically, the etching rate SiOF based on N_2 and O_2 is almost the same as that of SiO_2. The value of the etching rate of these two etching stop layers is near 100 Å/min, independent of the reactant gas ratio, rf power, and bias power. If the 1μm thickness of low-*K* materials such as *a*-C:F was adopted for interlayer dielectric films, the deposited thickness of the etching stop layer of SiOF and SiO_2 would be less than 50 nm. The effective dielectric constant of cap layers only increased 5%, and is verified by the experimental data. The defects of SiOF as an etching stop layer were due to stronger moisture absorption than SiO_2. This characteristic would cause the larger effective dielectric constant and degraded reliability. As our TDS and chemical mechanical polishing (CMP) experiments show in Figs. 10 and 11, the N_2O plasma treatment could enhance resistance to moisture absorption. Furthermore, the N_2O gas could be employed as an etching reactant gas of *a*-C:F. If the N_2O gas could be mixed with N_2 and O_2, a perfectly controlled trench profile with lower effective dielectric constant could be expected. Further efforts are currently underway.

TABLE I. Parameters for the damascene etch process.

Etching parameter		
Pressure	5 mTorr	5 mTorr
Temperature	60–70 °C	60–70 °C
Power	2000 W	2000 W
Bias	60 W	60 W
CHF_3	5 sccm	
CF_4	95 sccm	
N_2		80 sccm
O_2		20 sccm
Etching time	40 s	60–105 s

After the etching process, a damascene pattern of ~150 nm was employed for copper electroplating. Optimized copper electroplating electrolytes for 0.15 μm damascene features have been implemented, shown in Fig. 12. According to our research, the super filling phenomenon would apparently occur when wetting agents with two different molecular weights and a heterocyclic compound were present in the electrolyte.

IV. CONCLUSION

By analyzing film characteristics of *a*-C:F, the *a*-C:F films deposited by PECVD achieved high thermal stability (400 °C) and a low-dielectric constant ($K\sim2.3$). The dry etching of *a*-C:F was successfully demonstrated for the dimension below 150 nm. In our Damascene architecture, the etching stop layer or hard mask of both SiOF and SiO_2 was studied. The etch rate and etching rate selectivity were opti-

FIG. 9. SEM images of the etching profiles of *a*-C:F in O_2 plasmas (100 sccm) with bias power of 60 W (60 s).

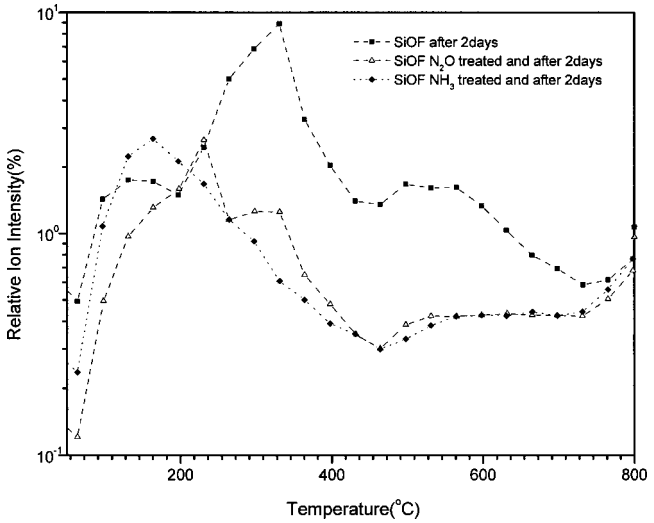

FIG. 10. TDS curves for SiOF for various plasma treatments and moisture environment tests.

mized by changing the content ratio between N_2 and O_2. Furthermore, the bias power, rf power, and gas flows were changed to control the etch profile. The SEM results showed that a better etch profile can be obtained at higher bias power. The distribution density of the reactant etching gas in the sub-μm gap, different from the blanket surface of the wafer, apparently caused reduction of the etching rate in the trenches/vias. Due to this phenomenon, the etching rate became a nonlinear function of the trench/via dimensions. An optimized copper electroplating electrolyte for the 0.15 μm Damascene feature was implemented. According to our research, the superfilling phenomenon would apparently occur

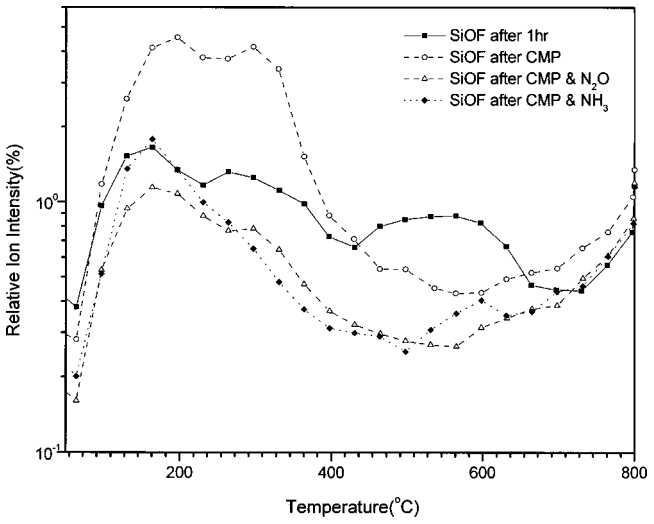

FIG. 11. TDS curves for SiOF for various plasma treatments and CMP processing.

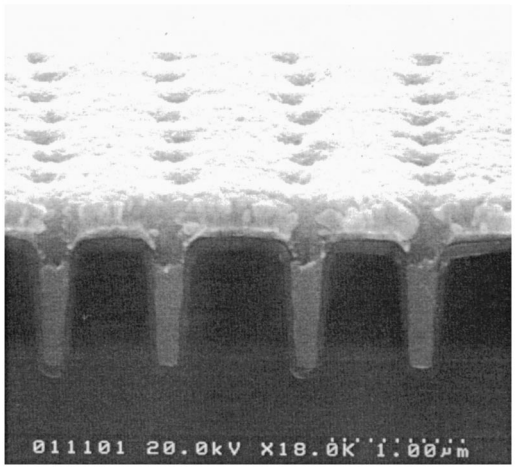

FIG. 12. Superfilling electroplating for a 6:1 AR, 0.15 μm via by adding a heterocyclic compound+complex wetting agents in a conventional electrolyte.

when wetting agents with two different molecular weights and a heterocyclic compound are present in the electrolyte.

ACKNOWLEDGMENTS

This work was sponsored by the National Science Council of the Republic of China under Grant No. NSC90-2721-2317-200. Technical support from Merck–Kanto Advanced Chemical Ltd. is also acknowledged.

[1]K. Kobayashi, A. Sano, H. Akahoshi, T. Itabashi, T. Haba, S. Fukada, and H. Miyazaki, IITC 2000 Conference, 2000, pp. 34–36.
[2]P. C. Andricacos *et al.*, IBM J. Res. Dev. **42**, 567 (1998).
[3]J. J. Kelly *et al.*, J. Electrochem. Soc. **146**, 2540 (1999).
[4]L. Peter, Semicond. Int. 64 (1998).
[5]W. W. Lee and P. S. Ho, MRS Bull. 19 (1997).
[6]N. P. Hacker, MRS Bull. 33 (1997).
[7]K. Endo, T. Tatsumi, Y. Matsubara, and T. Horiuchi, Jpn. J. Appl. Phys., Part 1 **37**, 1809 (1998).
[8]S. Baskaran, J. K. Domansky, N. Kohler, X. Li, C. Coyle, G. E. Fryxell, S. Thevuthasan, and R. E. Williford, Adv. Mater. **12**, 291 (2000).
[9]B. K. Hwang, M. J. Loboda, G. A. Cerny, R. F. Schneider, J. A. Seifferly, and T. Washer, in Ref. 1, p. 52.
[10]Y. Ma, H. Yang, J. Guo, C. Sathe, A. Agui, and H. Nordgren, Appl. Phys. Lett. **72**, 3353 (1998).
[11]I. Banerjee, M. Harker, L. Wong, P. A. Coon, and K. K. Gleason, J. Electrochem. Soc. **146**, 2219 (1999).
[12]K. Endo, K. Shinoda, and T. Tasumi, J. Appl. Phys. **86**, 2739 (1999).
[13]T. E. F. M. Standaert, P. J. Matsuo, S. D. Allen, G. S. Oehrlein, and T. J. Dalton, J. Vac. Sci. Technol. A **17**, 741 (1999).
[14]C. Janowiak, S. Ellingboe, and I. Morey, J. Vac. Sci. Technol. A **18**, 1859 (2000).
[15]M. R. Breen, C. M. Foster, S. Bass, J. J. Lee, and W. Mlynko, J. Vac. Sci. Technol. B **18**, 1314 (2000).
[16]M. R. Baklanov, S. Vanhaelemeersch, H. Bender, and K. Maex, J. Vac. Sci. Technol. B **17**, 372 (1999).
[17]M. R. Baklanov, M. Van Hove, G. Mannaert, S. Vanhaelemeersch, H. Bender, T. Conard, and K. Maex, J. Vac. Sci. Technol. B **18**, 1281 (2000).
[18]S. M. Han and E. S. Aydil, J. Appl. Phys. **83**, 2172 (1998).
[19]R. d'Agostino, F. Cramarossa, V. Colaprico, and R. d'Ettole, J. Appl. Phys. **54**, 1284 (1985).
[20]R. d'Agostino, F. Cramatossa, and S. De Benedictis, Plasma Chem. Plasma Process. **4**, 21 (1984).